Design and Implementation of a Bidirectional DC-DC Converter for Stand-Alone Photovoltaic Systems

[1*]Kuei-Hsiang Chao, [1]Ming-Chang Tseng, [1]Chun-Hao Huang, [2]Yang-Guang Liu

and [2]Liang-Chiao Huang

Abstract

In this study, we focused on developing a bidirectional power converter for a stand-alone photovoltaic power generation system and system energy management when a lithium-iron battery is used to regulate the power supply. We used a small-scale air-conditioner to provide the load for the bidirectional power converter developed in this study to examine the efficiency of the converter and the performance of energy management systems. The overall framework of the proposed system comprised a maximum power point tracking controller, bidirectional buck-boost converter, lithium-iron battery, small-scale air-conditioner, and energy management system. An energy management strategy was proposed to increase the power utilization rate of the photovoltaic power generation system. Some measurement results are made to verify the feasibility of an air conditioner system with a photovoltaic power generation system and lithium-iron battery hybrid power supply.

Keywords: photovoltaic (PV) generation system, small-scale air-conditioner, power management strategy, energy management strategy.

1. Introduction

As business and industrial requirements and people's needs increase, the demand for small-scale air-conditioners in general households and office spaces have risen dramatically. However, the greater power loads of small-scale air-conditioners have caused power companies to increase the reserve margin during peak power usage times in the summer. Therefore, using the energy produced by photovoltaic power systems effectively, many studies has been investigating the development of a photovoltaic power generation system with energy management properties for small-scale air conditioners and methods to reduce peak power loads [1-3]. Furthermore, identical to most renewable energy sources, photovoltaic power generation systems also provide a direct current (DC) power supply. Therefore, this research tends to enhancing the energy conversion efficiency of photovoltaic power generation systems by increasing the efficacy of photovoltaic power generation systems applied to small-scale air-conditioners, and supplied the DC power produced by photovoltaic power generation systems to inverter-fed small-scale air-conditioners [4-8].

The energy management framework of stand-alone photovoltaic power generation systems can provide a stable power supply for small-scale air-conditioners using a bidirectional buck-boost converter with battery charging and discharging characteristics. In the framework of general bidirectional buck-boost converters, the diode component of the boost converter is substituted with a power semiconductor switch. Consequently, a synchronous rectification framework and bidirectional energy flow characteristics are provided for the converter. The switch conduction losses can be reduced by applying a synchronous rectification framework [9-15] to increase the energy conversion efficiency provided for comparing to that of general boost converters.

To appropriately employ the power output of the photovoltaic power generation system, we combined the bidirectional buck-boost converter developed in this study with a lithium-iron rechargeable battery. Furthermore, we proposed a small-scale air-conditioner energy management strategy based on a hybrid power supply provided by a photovoltaic power generation system and lithium-iron rechargeable battery to increase the photovoltaic power generation system's stable supply of power.

*CorrespondingAuthor: Kuei-Hsiang Chao
(E-mail:chaokh@ncut.edu.tw).
[1] Department of Electrical Engineering, National Chin-Yi University of Technology, 57, Sec. 2, Zhongshan Rd., Taiping Dist., Taichung 41170, Taiwan
[2]Green Energy & Environmental Research Laboratories (GEL) of ITRI , Taiwan

2. System Framework

Figure 1 shows the power converter system framework of the stand-alone photovoltaic power generation system [16]. This framework combines a maximum power point tracking controller and a bidirectional buck-boost converter equipped with a charge and discharge control function. The battery charge and discharge controller employ a bidirectional buck-boost converter that simultaneously exhibits the energy conversion characteristics of buck and boost converters. Thus, the energy conversion efficiency is significantly increased. Furthermore, this converter in the system framework provides not only battery energy storage functions, but also facilitates auxiliary power supply at the load terminal. By implementing the system characteristics are mentioned previously, the power supply can be managed and controlled.

The maximum power point tracking controller is focused on tracking and controlling the output power of the photovoltaic module array. Therefore, the system's DC link voltage (V_H) varies according to solar irradiation and tracking processes. If V_H is directly connected to the load terminal system, the system will become compromised. Therefore, we proposed a control strategy that allowed V_H to be controlled at a 350V setting through the charge and discharge control function of a bidirectional buck-boost DC-DC converter. The control method involves adopting the error between of the DC link voltage V_H and its command value (V_H^*) to further obtain the battery charge/discharge current command value (I_o^*) through the DC link voltage controller. Subsequently, the hysteresis current controller senses the charge and discharge current (I_L) of the battery to follow its command value to achieve DC link voltage (V_H) regulatory functions. Additionally, to prevent excessive I_L, the system restricts the maximum charging current. Therefore, when the charging current exceeds the default value, the system discontinues the maximum power tracking procedure to protect the battery from damage. This control strategy enables the photovoltaic module array to maintain a maximum power output under various solar irradiation intensities. Additionally, the DC link control strategy is employed to achieve DC link voltage (V_H) control. Furthermore, the control system adopts proportional-integral controllers (PI controllers) that are easily implemented. The parameters of the DC link voltage controller are K_{Pv} = 0.5 and K_{Iv} = 0.008, and the parameters of the hysteresis current controller are K_{Pi} = 0.1 and K_{Ii} = 0.001.
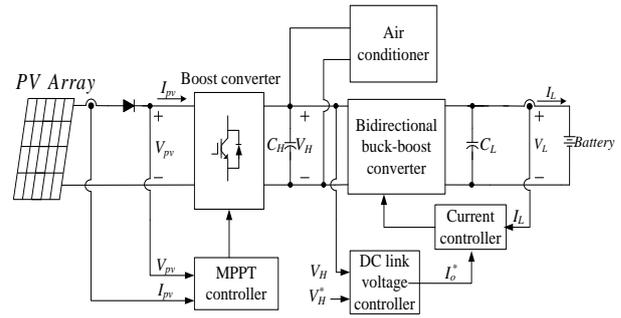
Figure 1: System framework of the photovoltaic power generation system applied to small-scale air-conditioners

3. The Proposed Bidirectional Buck-Boost Converter

To facilitate power storage generated from stand-alone photovoltaic power generation systems during overproduction, it provides the stored power as an auxiliary service during electricity shortages. This study proposes a bidirectional buck-boost converter (as shown in Figure 2) [17] to manage the storage and supply of power between photovoltaic power generation systems and batteries. Due to the circuit structure of a bidirectional converter allows bidirectional power flows, two operation modes can be set for this converter depending on the direction of the power flow: boost and buck modes. The following section provides in-depth descriptions regarding the fundamental topology and component design of the proposed bidirectional buck-boost converter circuit.
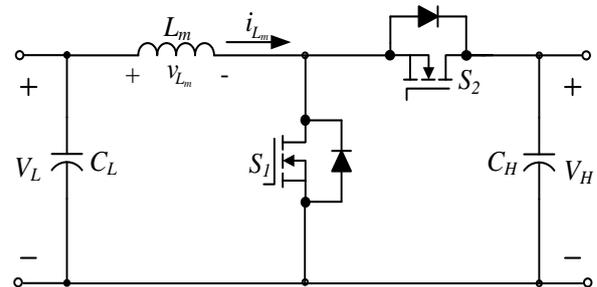
Figure 2: Framework for the bidirectional buck-boost converter circuit

3.1 Boost Mode

The proposed converter circuits possess two operational modes depending on the switch motion in the switch-mode power supply (SMPS): open and closed. Subsequently, in a single operation cycle, the converter's duty cycle D is defined as the ratio of the close duration of the switch to period T, as shown in (1) [16-18].

$$D = \frac{t_{on}}{T} = \frac{t_{on}}{t_{on} + t_{off}} \tag{1}$$

Where t_{on} and t_{off} respectively represent the close and open durations of the switch in a single operation cycle.

The following section provides in-depth descriptions regarding the principles of operation and component designs of the proposed bidirectional buck-boost converter operating under boost mode.

1).Closed switch S_1 ($0 \leq t < DT$)

When switch S_1 on the low-voltage side of the converter is closed, switch S_2 on the high-voltage side presents an opened state because of the complementary mechanism between the switches on the high-voltage and low-voltage sides. Consequently, the converter becomes an equivalent circuit, as shown in Figure 3. In this mode, the inductor L_m and low-voltage supply V_L connect in parallel, causing the inductor voltage v_{Lm} and voltage V_L on low-voltage side to be equal. The circuit equation can be expressed as

$$v_{Lm} = V_L = L_m \frac{di_{Lm}}{dt} \tag{2}$$

The rate of change in the inductor voltage i_{Lm} is constant. Therefore, the inductor current presents a linear increase when the switch is closed. The change of the inductor current can be expressed as

$$\frac{\Delta i_{Lm}}{\Delta t} = \frac{\Delta i_{Lm}}{DT} = \frac{V_L}{L_m} \tag{3}$$

From (3), the following can be obtained:

$$\Delta i_{Lm(on)} = \frac{V_L}{L_m} DT \tag{4}$$
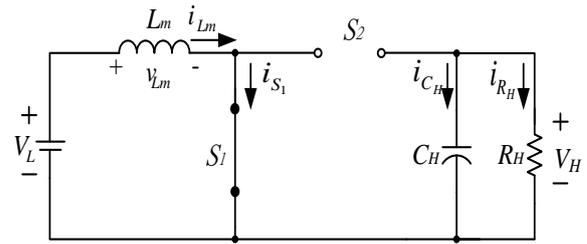
Figure 3: The equivalent circuit of the proposed bidirectional buck-boost converter operating under boost mode and when the switch S_1 on the low-voltage side is closed

2).Open switch S_1($DT \leq t < T$)

When switch S_1 on the low-voltage side of the converter is in an open mode, switch S_2 on the high-voltage side presents a closed state. The equivalent circuit for the converter is shown in Figure 4. The inductor voltage v_{Lm} for this state can be expressed as

$$v_{Lm} = V_L - V_H = L_m \frac{di_{Lm}}{dt} \tag{5}$$

Simplifying (5), the following equation is obtained:

$$\frac{di_{Lm}}{dt} = \frac{V_L - V_H}{L_m} \tag{6}$$

When the switch S_1 is open, the change of the inductor voltage i_{Lm} presents a linear decrease. This state can be express as

$$\frac{\Delta i_{Lm}}{\Delta t} = \frac{\Delta i_{Lm}}{(1-D)T} = \frac{V_L - V_H}{L_m} \tag{7}$$

From (7), the following equation can be obtained:

$$\Delta i_{Lm(off)} = \frac{(V_L - V_H)}{L}(1-D)T \tag{8}$$
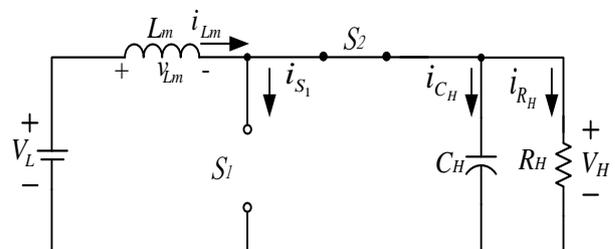
Figure 4: The equivalent circuit of the proposed bidirectional buck-boost converter operating under boost mode and when the switch S_1 on the low-voltage side is opened

Under a steady-state operation, the change of the converter's inductor current i_{Lm} in a single cycle of operation must equal zero, that is,

$$\Delta i_{Lm(on)} + \Delta i_{Lm(off)} = 0 \qquad (9)$$

By incorporating (4) and (8) into (9), the following can be obtained:

$$\frac{V_L}{L_m}DT + \frac{(V_L - V_H)}{L_m}(1-D)T = 0 \qquad (10)$$

Simplifying (10), the following equation is obtained:

$$V_L DT + (V_L - V_H)(1-D) = 0 \qquad (11)$$

This equation represents the concept of the volt-second balance principle. In addition, by further simplifying (11), the voltage relationship between the low-voltage and high-voltage sides of the converter for this operation mode can be determined as

$$V_H = \frac{1}{1-D}V_L \qquad (12)$$

As shown in (12), $0 \le D \le 1$. Therefore, the voltage V_H on the high-voltage side is greater than the voltage V_L on the low-voltage side.

3). Component designs of the converter operating under boost mode

  (i) The capacitance design

The above analysis was conducted under the assumption that the value for capacitor C_H was *ad infinitum,* and thus capable of maintaining the voltage V_H on the high-voltage side of the converter at a steady value. Actually, the voltage V_H on the high-voltage side varies because of a limiting capacitor. Subsequently, the variable charges on capacitor C_H are as follows:

$$\left| \Delta Q_H \right| = \frac{V_H}{R_H}DT = C_H \Delta V_H \qquad (13)$$

From (13), the ripple voltage can be expressed as

$$\Delta V_H = \frac{V_H DT}{R_H C_H} = \frac{V_H D}{R_H C_H f} \qquad (14)$$

Simplifying (14), the following equation is obtained

$$C_H = \frac{D}{R_H f(\Delta V_H / V_H)} \qquad (15)$$

Where R_H is the equivalent load resistance on the high-voltage side, f is the switching frequency of the converter, and $\Delta V_H / V_H$ is the ripple ratio of the voltage on the high-voltage side.

(ii) The inductance design

Neglecting line loss, the input power P_L of the converter on the low-voltage side should be equivalent to the output power P_H on the high-voltage side. Subsequently, the following can be obtained:

$$V_L I_{Lm} = \frac{V_H^2}{R_H} = \frac{(V_L/(1-D))^2}{R_H} = \frac{V_L^2}{(1-D)^2 R_H} \qquad (16)$$

Thus, mean value I_{Lm} of the inductor current can be obtained

$$I_{Lm} = \frac{V_L}{(1-D)^2 R_H} \qquad (17)$$

The maximum and minimum values for the inductor current can be obtained through (4) and (17).

$$I_{Lm\_max} = I_{Lm} + \frac{\Delta i_{Lm}}{2} = \frac{V_L}{(1-D)^2 R_H} + \frac{V_L}{2L_m}DT \qquad (18)$$

$$I_{Lm\_min} = I_{Lm} - \frac{\Delta i_{Lm}}{2} = \frac{V_L}{(1-D)^2 R_H} - \frac{V_L}{2L_m}DT \qquad (19)$$

For the inductor current to operate under a continuous conduction mode (CCM), the minimum value of the inductor current must be greater than zero. Thus, (19) must be satisfied

$$\frac{V_L}{(1-D)^2 R_H} - \frac{V_L}{2L_m}DT \ge 0 \qquad (20)$$

Simplifying (20), any facilitating the inductor current to operate under a CCM, the minimum inductor current value must be satisfied

$$L_{m,min} \ge \frac{D(1-D)^2 R_H}{2f} \qquad (21)$$

Therefore, the proposed bidirectional buck-boost converter to operate in boost mode simultaneously maintains inductor current operations in CCM in any duty cycle. The duty cycle in which the $L_{m,min}$ of (21) possesses the maximum value must first be determined. Subsequently, the D value is increased from 0 to 1 in increments of 0.005. These values are incorporated into function $D(1-D)^2$ of (21), as shown in Figure 5. It is seen in Figure 5 that when $D=1/3$, the function

achieves the maximum value solution. Therefore, when designing the inductance value, the *D* value is substituted with 1/3, and the product is multiplied by 1.25. This process ensures that the inductor current can be operated under CCM in any duty cycle.

3.2 Buck Mode

The following section provides in-depth descriptions regarding the principles of operation and component designs of the proposed bidirectional buck-boost converter operating under buck mode.

1).Closed switch S_2 ($0 \le t \le DT$)

When switch S_2 on the high-voltage side of the converter is closed, switch S_1 on the low-voltage side presents an opened state because of the complementary mechanism between the signals controlling the switches on the low-voltage and high-voltage sides. Subsequently, the converter in this state becomes an equivalent circuit, as shown in Figure 6. The voltage on both ends of inductor component L_m can be expressed as follows:

$$v_{Lm} = V_H - V_L = L_m \frac{di_{Lm}}{dt} \qquad (22)$$

Simplifying (22), the following equation is obtained:

$$\frac{di_{Lm}}{dt} = \frac{V_H - V_L}{L_m} \qquad (23)$$

During this operation mode, the rate of change for the inductor current is a positive value, thus, presenting a linear increase. When the switch is closed, the change of the inductor current in (23) can be rewritten as

$$\frac{\Delta i_{Lm}}{\Delta t} = \frac{\Delta i_{Lm}}{DT} = \frac{V_H - V_L}{L_m} \qquad (24)$$

From (24), the following can be obtained:

$$\Delta i_{Lm(on)} = \frac{(V_H - V_L)}{L_m} DT \qquad (25)$$

2). Open switch S_2 ($DT \le t \le T$)

When switch S_2 on the high-voltage side of the converter is open, switch S_1 on the low-voltage side presents a closed state. The equivalent circuit for the converter is shown in Figure 7, and the voltage at both ends of the inductor can be expressed as

$$v_{Lm} = -V_L = L_m \frac{di_{Lm}}{dt} \qquad (26)$$
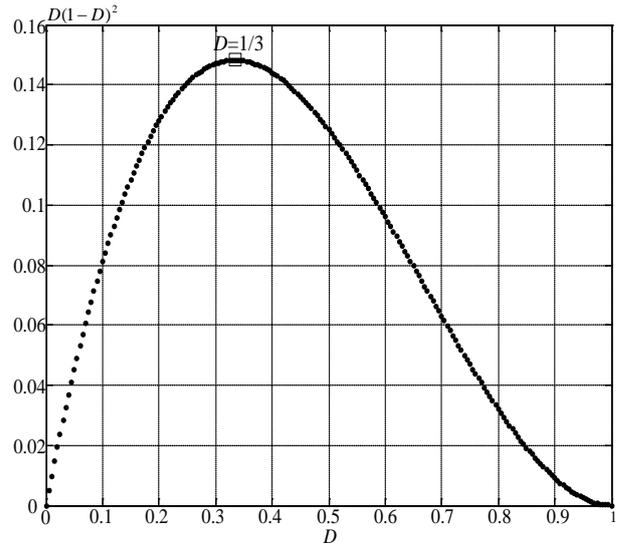
Figure 5: A diagram of function $D(1-D)^2$
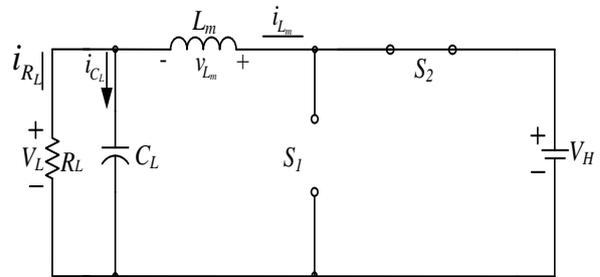
Figure 6: The equivalent circuit of the proposed bidirectional buck-boost converter operating under buck mode and when the switch S_2 on the high-voltage side is closed

Simplifying (26), the following equation is obtained:

$$\frac{di_{Lm}}{dt} = \frac{-V_L}{L_m} \qquad (27)$$

In this operation mode, the rate of change of the inductor current is a negative value, thus, presenting a linear decreased. When the switch is closed, the change in the inductor current in (27) can be rewritten as

$$\frac{\Delta i_{Lm}}{\Delta t} = \frac{\Delta i_{Lm}}{(1-D)T} = -\frac{V_L}{L_m} \qquad (28)$$

From (28), the following can be obtained:

$$\Delta i_{Lm(off)} = -\frac{V_L}{L_m}(1-D)T \qquad (29)$$
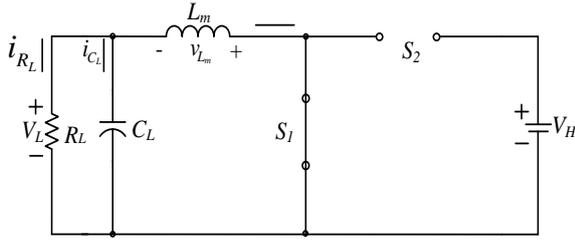
Figure 7: The equivalent circuit of the proposed bidirectional buck-boost converter is operated under buck mode when the switch S_2 on the high-voltage side is open

Under steady-state operation, the net change of the converter's inductor current in a single cycle of operation must equal zero, thus

$$\Delta i_{Lm(on)} + \Delta i_{Lm(off)} = 0 \qquad (30)$$

From (25) and (29), the following equation can be obtained:

$$\frac{(V_H - V_L)}{L_m}DT - \frac{V_L}{L_m}(1-D)T = 0 \qquad (31)$$

Simplifying (31), the following equation is obtained:

$$(V_H - V_L)DT - V_L(1-D)T = 0 \qquad (32)$$

This equation represents the volt-second balance principle. In addition, by further simplifying (32), the voltage relationship between the high-voltage and low-voltage sides of the converter for this operation mode can be determined as

$$V_L = V_H D \qquad (33)$$

As shown in (33), $0 \le D \le 1$. Therefore, under this operation mode, the voltage V_L on the low-voltage side is smaller than the voltage V_H on the high-voltage side.

3). Component designs of the converter are operated under buck mode:
(i)The capacitance design
As shown in Figure 8, the currents for capacitor C_L are as follows:

$$i_{CL} = i_{Lm} - i_{RL} \qquad (34)$$

In addition, Figure 8 shows that, when capacitor current i_{CL} is a positive value and the capacitor undergoes charging, the capacitance and the output voltage on the low-voltage side can be defined the changes of the capacitor charges as

follows:

$$\Delta Q_L = C_L \Delta V_L \qquad (35)$$

In addition, the solution for (35) can be obtained by calculating the area of the positive capacitor current value presented in Figure 8.

$$\Delta Q_L = \frac{T\Delta i_{Lm}}{8} \qquad (36)$$

Simplifying (35) and (36), the voltage rippled on the low-voltage side can be expressed as

$$\Delta V_L = \frac{T\Delta i_{Lm}}{8C_L} \qquad (37)$$

Subsequently, by incorporating (29) into (37), the following equation is obtained:

$$\Delta V_L = \frac{V_L(1-D)}{8C_L L_m f^2} \qquad (38)$$

Where $f \stackrel{\Delta}{=} 1/T$ is the switching frequency of the converter.
Therefore, (38) formulates the following equayion:

$$C_L = \frac{(1-D)}{8(\Delta V_L / V_L)L_m f^2} \qquad (39)$$
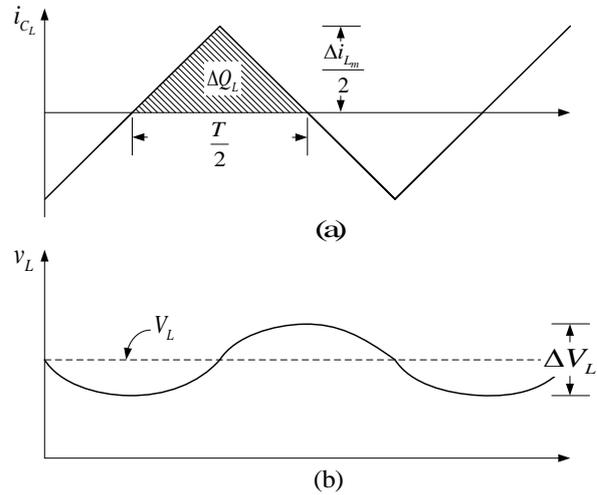
Figure 8: The waveforms of the bidirectional buck-boost converter operating under buck mode：(a)the current of the capacitor; (b)the voltage ripple of the capacitor on the low-voltage side

According to the specification requirements of output voltage ripple $\Delta V_L / V_L$,

the size of the output capacitor value on the low-voltage side can be determined.

(ii)The inductance design

When the bidirectional buck-boost converter operates under buck mode, the mean of capacitor current and the mean current flow through load resistor R_L are identical because the mean value of the capacitor current under steady operation is zero. Thus, the mean value can be expressed as follows:

$$I_{Lm} = I_{RL} = \frac{V_L}{R_L} \qquad (40)$$

Furthermore, the maximum and minimum values for the inductor current can be obtained through (25) and (29), respectively.

$$I_{Lm\_max} = I_{Lm} + \frac{\Delta i_{Lm}}{2}$$
$$= \frac{V_L}{R_L} + \frac{1}{2}\left[\frac{V_L}{L_m}(1-D)T\right] = V_L\left[\frac{1}{R_L} + \frac{(1-D)}{2L_m f}\right] \qquad (41)$$

$$I_{Lm\_min} = I_{Lm} - \frac{\Delta i_{Lm}}{2}$$
$$= \frac{V_L}{R_L} - \frac{1}{2}\left[\frac{V_L}{L_m}(1-D)T\right] = V_L\left[\frac{1}{R_L} - \frac{(1-D)}{2L_m f}\right] \qquad (42)$$

For the inductor current to operate under a CCM, the minimum value of the inductor current must be greater than zero. Thus, the following is obtained from (42):

$$V_L\left[\frac{1}{R_L} - \frac{(1-D)}{2L_m f}\right] \geq 0 \qquad (43)$$

Thus, according to (43), to facilitate the continuity of the inductor current under buck mode, the minimum inductance must be satisfied.

$$L_{m\_min} \geq \frac{(1-D)R_L}{2f} \qquad (44)$$

To maintain the consistency of the inductor current flows for the bidirectional buck-boost converter when operating under boost and buck modes, (21) and (44) can be further simplified as follows:

$$L_{m\_boost} = \frac{D(1-D)^2 V_H^2}{2P_H f} \qquad (45)$$

$$L_{m\_buck} = \frac{(1-D)V_L^2}{2P_L f} \qquad (46)$$

Where $P_H = V_H^2 / R_H$ and $P_L = V_L^2 / R_L$. Assuming that the D value is increased

from 0 to 1 in increments of 0.005, these values can then be substituted into function $D(1-D)^2 V_H^2$ of (45) and function $(1-D)V_L^2$ of (46). Furthermore, DC link voltage V_H (on the high-voltage side) for the proposed converter is established as 350 V, and battery voltage V_L (on the low-voltage side) is set at 96 V. Consequently, a diagram can be drafted by using these two functions (Figure 9). As shown in Figure 9, when D=1/3, function $D(1-D)^2 V_H^2$ achieves the maximum value solution, and this value is greater than $(1-D)V_L^2$ in any duty cycle, indicating that is under any duty cycle.

$$\frac{D(1-D)^2 V_H^2}{2P_H f} \geq \frac{(1-D)V_L^2}{2P_L f} \qquad (47)$$

Therefore, to maintain the consistency of the inductor current flow for the bidirectional buck-boost converter when operating under boost or buck modes, the D value is substituted with 1/3 when designing the inductance value of the bidirectional buck-boost converter. Subsequently, the product is multiplied by 1.25. This process ensures that the inductor current can operate under CCM.

3.3 The Component Designs for the Bidirectional Buck-Boost Converter

The modes of operation for the bidirectional buck-boost converter have been explained in Sections 3.1 and 3.2. In the following sections, the previously obtained analysis results are used to design the components of the proposed converter. The electrical specifications and parameters of the proposed converter are shown in Table 1.
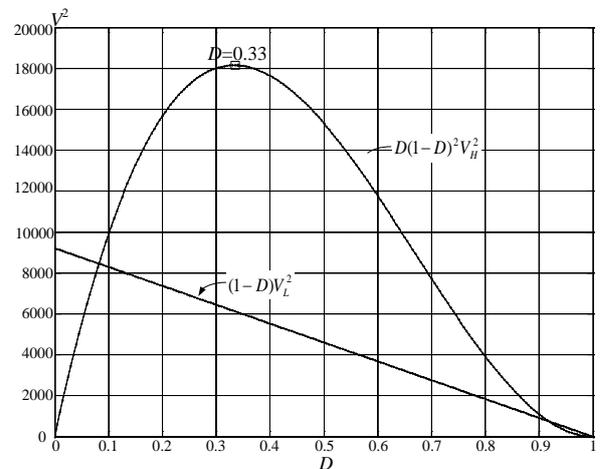
Figure 9:The diagram of the $D(1-D)^2 V_H^2$ and $(1-D)V_L^2$ functions

Table 1. The electrical specifications of the bidirectional buck-boost converter

DC link voltage, V_H (on the high-voltage side)	$V_H = 350V$
Battery voltage, V_L (on the low-voltage side)	$V_L = 96V \pm 10\%$
Switching frequency, f	$f = 16kHz$
Maximum operation power, P_{max}	$P_{max} = 1200W$

The mentioned component designs for the proposed converter are explained as follows.

1).Inductance component design

The bidirectional buck-boost converter design proposed in this study facilitates the inductor current in operating under a discontinuous conduction mode during light-load periods and under CCM during heavy-load periods. This design reduces the conduction losses induced by switching under light-load periods and maintains current continuity during heavy-load periods to reduce current peak values [15]. The inductance value can be obtained through (45) and expressed as follows:

$$L_{m(min)} = \frac{D(1-D)^2 V_H^2}{2P_C f} = 1.89(mH) \qquad (48)$$

Where duty cycle D is 1/3, the voltage V_H on the high-voltage side is 350V, and critical light-load power P_C is 300 W. Furthermore, to ensure that the converter maintains operations under CCM, even when the load power exceeds the critical light-load power, the inductance was set at 2.5 *mH*.

2).Capacit deign on both sides

The primary consideration for selecting the C_H capacitor on the high-voltage side and capacitor C_L on the low-voltage side was the size of the output voltage ripple required by the converter. Subsequently, the design method for the high-voltage side can be obtained through (15), and the low-voltage side can be obtained through (39), consequently selecting $C_H = C_L = 460\,\mu F$.

3). Switch component design

Based on previous analyses, the maximum current flowing through the main switch components can be obtained through (18) or (41). Simplifying (41), the following is obtained:

$$I_{Lm\_max} = V_L \left[\frac{P_{max}}{V_L^2} + \frac{(1-D)}{2L_m f} \right] = 13.376A \qquad (49)$$

These analysis indicate that the maximum voltage load is accepted by the main switches is 350 *V*. Considering

the actual experimentation, the switching modes on hard switching structures can cause excessive, instantaneous voltage and current surges that damage switch components. Therefore, the IPW90R120 (36A/900V) switch component was selected.

4. Measured Results of the Air Conditioner System

To verify the energy regulation properties of the stand-alone photovoltaic power generation system's framework is under various loads and solar irradiation changes. We combined a bidirectional buck-boost converter and a maximum power point tracking controller in a stand-alone photovoltaic power generation system framework, as shown in Figure 10. In addition, we used an inverter-fed air-conditioner to provide the applied load. To facilitate indoor measurements, the simulator E4360A [19] manufactured by the Agilent Technologies Company was adopted for the photovoltaic module array to substitute the HIP230HDE1 photovoltaic module [20]. We adopted a 920 W system established through a 4-series and 1 parallel connection scheme. Furthermore, to facilitate real-time monitoring of the proposed system's operation, we developed a monitoring interface (shown in Figure 11) that could instantly monitor the photovoltaic module array, battery terminal, and air-conditioner operations.

We adopted a solar irradiation to change in the beginning at 750 W/m^2 and decline to 350 W/m^2, and then increase to 750 W/m^2 for loading requirements in which the set air conditioner temperature differed from the surrounding environment by 1°C and 3°C to test the power supply efficacy of the photovoltaic power generation system. Figure 12 shows the DC link voltage (V_H), battery voltage (V_L), and battery current (I_L) changes under an air-conditioner setting of a 1°C that is different from the surrounding environment and a solar irradiation intensity change beginning 750 W/m^2, declining to 350 W/m^2, and then increasing to 750 W/m^2. The results in Figure 12 show that with a 750 W/m^2 irradiation, the system enters a charge mode to maintain a 350 V DC link voltage (V_H) because the air-conditioner power demand is 450 W, which is less than the output power of the photovoltaic module array. When the irradiation is reduced to 350 W/m^2, the photovoltaic module array cannot supply sufficient energy for small-scale air-conditioners. Therefore, the formulated DC link voltage (V_H) regulation strategy enables the system to adopt the auxiliary power supply mode, which rapidly regulates the DC link voltage (V_H) to the set value (350 V).

To verify that the power converter framework

of the stand-alone photovoltaic power generation system can achieve identical power regulation performances under various air-conditioner load changes, we adopted an air-conditioner temperature setting of a 3°C difference from the surrounding environment as the load change condition. Additionally, the power consumption of the air-conditioner was set as 1,100W. The test waveform of this load under irradiation intensity that begins at 750 W/m², decline to 350 W/m², and increases to 750 W/m² as shown in Figure 13. The measurement results indicated that although the irradiation produced significant changes during tests with various loads, the framework proposed in this study rapidly regulates the DC link voltage (V_H) and maintains a stable power supply. The main reason for this result was the adoption of a lithium-iron rechargeable battery with rapid charging and discharging characteristics in the energy regulation framework. Therefore, the framework can rapidly switch between charge and auxiliary power supply modes to regulate energy without damaging the battery terminal.
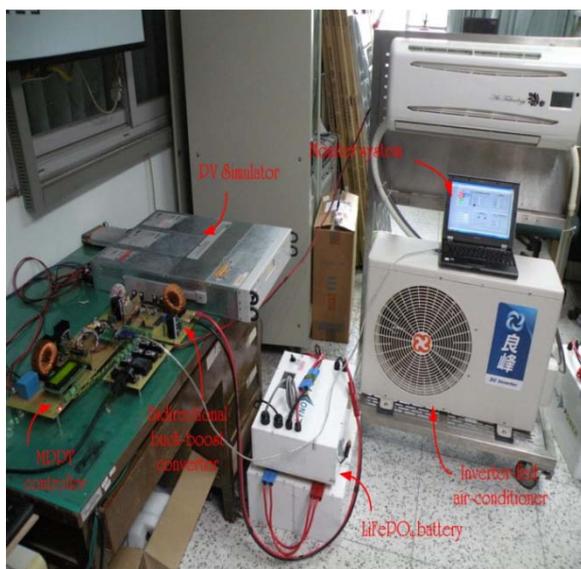
Figure 10: The framework of the stand-alone photovoltaic power generation system

The tests mentioned above were only employed to examine the energy regulation of the framework based on solar irradiation changes under fixed air-conditioner loads. To further assess the performance of the framework, we examined the power regulation of the energy management system under the fixed solar irradiation and significantly various air-conditioner power demands. Figures 14-15 show the measured V_H, V_L, and I_L changes under a 600 W/m² irradiation and a set air-conditioner temperature difference from the surrounding environment that increased from 0°C to 3°C, and declined from 3°C to 0°C. The set air-conditioner temperature difference is identified to the load power

consumption increased from 50W to 1,100W, and decreased from 1,100 W to 50 W. The figures show that in despite of significant changes in load demands, the converter remained to be able to rapidly regulate the DC link voltage (V_H) by controlling the battery I_L, enabling stable power supply.
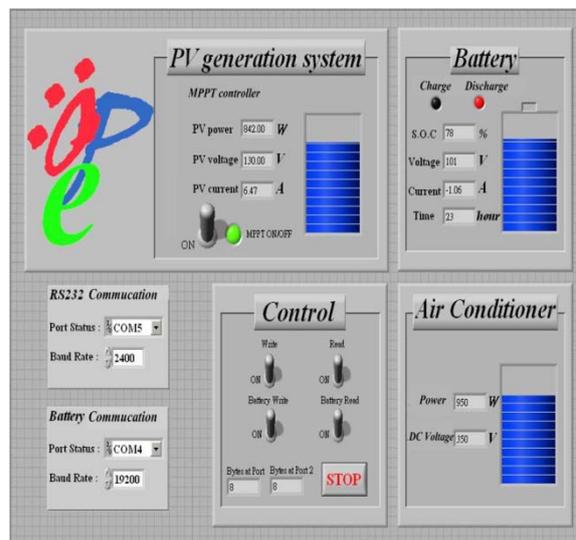
Figure 11: The monitoring interface system
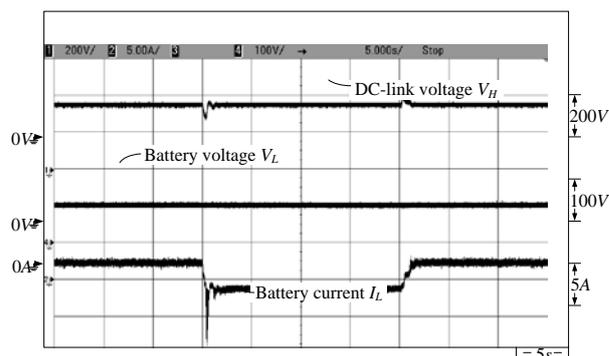
Figure 12: Changes in the V_H, V_L, and I_L under an air-conditioner setting of a 1°C difference from the surrounding environment (equivalent to a load power of 450W), and a solar irradiation change beginning at 750 W/m², declining to 350W/m², and increasing to 750 W/m²

Figures 14-15 also show that during the significant changes in the air-conditioner load power demands, the I_L does not directly achieve the corresponding charge and discharge current value. Instead, it operates at a specific current value for duration of time before gradually reaching the corresponding charge and discharge current of the specific load in the test. This is primarily caused by air-conditioner manufacturers delaying the compressor response time to extend its lifecycle. Through simulations and measurements, we verified

that using the DC link voltage and battery current controller to regulate the charge and discharge I_L enables of the power converter framework of the stand-alone photovoltaic power generation system to rapidly regulate the photovoltaic module array output power. This facilitates the storage of energy when an excess photovoltaic power generation is produced. In addition, when the load terminal power demand is greater, the battery is used to supply auxiliary power through the bidirectional converter's bidirectional energy flow characteristic. Furthermore, the DC link voltage (V_H) is also regulated, it ensures a stable supply of sufficient energy for small-scale air-conditioners under various irradiation and load changes. Online test results also verify that the power converter enhances the power generation efficiency and power supply's stability of photovoltaic power generation systems.
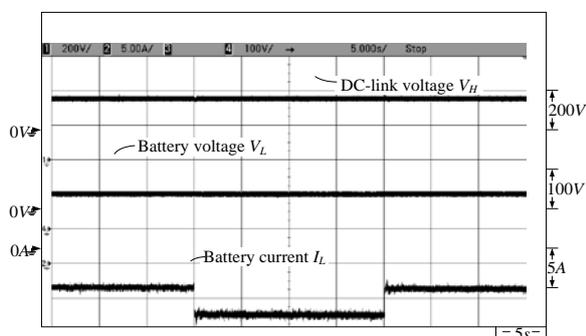
Figure 13: Changes in the V_H, V_L, and I_L under an air-conditioner setting of a 3°C difference from the surrounding environment (equivalent to a load power of 1,100W), and a solar irradiation change beginning at 750 W/m², declining to 350W/m², and increasing to 750 W/m²
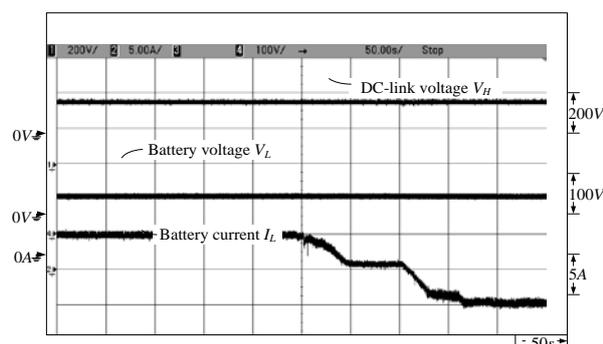
Figure 14: Changes in the V_H, V_L, and I_L under a 600W/m² irradiation and a set air-conditioner temperature difference from the surrounding environment that increased from 0 °C (load power = 50 W) to 3 °C (load power = 1,100 W)
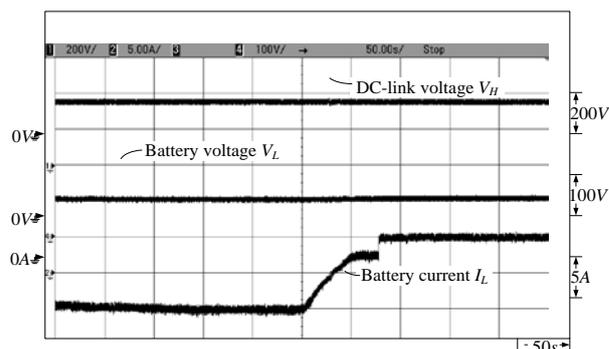
Figure 15: Changes in the V_H, V_L, and I_L under a 600W/m² irradiation and a set air-conditioner temperature difference from the surrounding environment that increased from 3 °C (load power =1,100W) to 0 °C (load power = 50 W)

5. Conclusion

In this study, we proposed a stand-alone photovoltaic power generation system framework for small-scale air-conditioners, and formulated a DC link voltage regulation strategy based on a bidirectional buck-boost converter combined with the charge and discharge functions of a battery. The DC link voltage not only maintains its set command value, but also supplies sufficient power for small-scale air-conditioners under insufficient irradiation through the charge and discharge functions of the battery. When higher levels of solar irradiation are provided, the excess energy is stored in the battery.

Acknowledgments

References

[1] ESTIF, "Sun in action II – A solar thermal strategy for Europe," 2003.

[2] ESTIF, "Solar thermal markets in Europe (Trends and Market Statistics 2004)," 2005.

[3] H. M. Henning, "Solare klimatisierung von gebäuden – eine Übersicht," erneuerbare energie, 2002.

[4] H. Kakigano, M. Nomura, and T. Ise, "Loss evaluation of DC distribution for residential houses compared with AC system," in

Proceedings of International Power Electronics Conference, pp. 480-486, 2010.

[5] F. Wicks, "Evaluating alternatives for integrating distributed DC generation with AC power systems," in Proceedings of the 35th Intersociety Energy Conversion Engineering Conference and Exhibition, vol. 2, pp. 763-766, 2000.

[6] K. H. Edelmoser, and F. A. Himmelstoss, "Bidirectional DC-to-DC converter for solar battery backup applications," in Proceedings of IEEE 35th Annual Power Electronics Specialists Conference, pp. 2070-2074, 2004.

[7] M. Suetomi, D. Imamichi, S. Matsumoto, D. Ueda, J. R. Yang, Y. Ishizuka, W. G. Lin, and H. Matsuo, "A novel bidirectional DC-DC converter with high power efficiency for isolation in high voltage DC power feeding systems," in Proceedings of IEEE 33rd International Telecommunications Energy Conference, pp. 1-4, 2011.

[8] M. Kumar, S. N. Singh, and S. C. Srivastava, "Design and control of smart DC microgrid for integration of renewable energy sources," in Proceedings of IEEE Power and Energy Society General Meeting, pp. 1-7, 2012.

[9] W. A. Tabisz, F. C. Lee, and D. Y. Chen, "A MOSFET resonant synchronous rectifier for high-frequency DC/DC converters," in Proceedings of IEEE PESC'90 Conference, pp. 769-779, 1990.

[10] M. Rodriguez, D. G. Lamar, M. A. Perez, D. Azpeitia, R. Prieto, and J. Sebastian, "A novel adaptive synchronous rectification system for low output voltage isolated converters," IEEE Transactions on Industrial Electronics, vol. 58, pp. 3511-3520, 2011.

[11] S. P. Yang, J. L. Lin, and S. J. Chen, "A novel ZCZVT forward converter with synchronous rectification," IEEE Transactions on Power Electronics, vol. 21, pp. 912-922, 2006.

[12] F. Weiyi, F. C. Lee, P. Mattavelli, and H. Daocheng, "A universal adaptive driving scheme for synchronous rectification in LLC resonant converters," IEEE Transactions on Power Electronics, vol. 27, pp. 3775-37781, 2012.

[13] W. Z. Zhong, W. P. Zhong, W. W. C. Ho, and S. Y. Hui, "Generalized self-driven AC–DC synchronous rectification techniques for single- and multiphase systems," IEEE Transactions on Industrial Electronics, vol. 58, pp. 3287-3297, 2011.

[14] H. J. Chiu, and L. W. Lin, "A bidirectional DC-DC converter for fuel cell electric vehicle driving system," IEEE Transactions on Power Electronics, vol.21, pp. 950-958, 2006.

[15] L. Y. Chang, K. H. Chao, and T. C. Chang, "Application of high voltage ratio and low ripple interleaved DC-DC converter for a fuel cell,"

The Scientific World Journal-Electronics, Article ID 896508, pp. 1-11, 2012.

[16] K. H .Chao, C. H. Huang, and Y. C .Chang, "Application of a photovoltaic generation system in a small-scale air conditioner," International Review of Electrical Engineering, vol. 7, no. 5, pp. 5927-5938, 2012.

[17] D. W. Hart, "Introduction to power electronics," Prentice, Prentice-Hall of USA, New York, 2003.

[18] K. H. Chao, R. H. Lee, and K. L. Yen, "Design of a hybrid power fed-converter and time controller for LED traffic light systems," International Review of Electrical Engineering, vol. 6, no. 3, pp. 1086-1093, 2010.

[19] PV simulator-E4360A specifications,

[20] http://www.home.agilent.com/agilent/product.js px?cc=TW&lc=cht&ckey=1370006&nid=-3548 9.771280.00&id=1370006&pselect=SR.GENER AL.

[21] SANYO photovoltaic module HIP-230HDE1 specifications, http://www.glea.pt/downloads/painel_fotovoltaic o_sanyo_220w.pdf.

Kuei-Hsiang Chao was born in Tainan, Taiwan, in 1962. He received the B.S. degree in electrical engineering from National Taiwan Institute of Technology, Taipei, Taiwan, in 1988, and the M.S. and Ph.D. degrees in electrical engineering from National Tsing Hua University, Hsinchu, Taiwan, in 1990 and 2000, respectively. He is presently a Professor at National Chin-Yi University of Technology, Taichung, Taiwan. His areas of interest are computer-based control system, applications of control theory, renewable energy and power electronics. Dr. Chao is a life member of the Solar Energy and New Energy Association and a member of the IEEE.

Ming-Chang Tseng was born in Kaohsiung, Taiwan, in 1988. He received the B.S. degree in electrical engineering from Cheng Shiu University of Technology, Kaohsiung, Taiwan, in 2010. He is currently a graduate student in the Department of Electrical Engineering of National Chin-Yi University of Technology. His research interests include photovoltaic power system, and power electronics design.

Chun-Hao Huang was born in Changhua, Taiwan, in 1988. He received the B.S. degree in electrical engineering from National Chin-Yi University of Technology, Taichung, Taiwan, in 2010. He is currently a graduate student in the Department of Electrical Engineering of National Chin-Yi University of Technology. His research interests include photovoltaic power system, and power electronics design.

Yang-Guang Liu received his Ph.D degree in Mechanical Engineering at National Chiao Tung University, Taiwan on 2010. At the same year, he joined the Environment Laboratories of ITRI in Hsinchu, Taiwan. Dr. Liu focused his research on CAE analysis, programming, mechanical design, power electronics and software development.

Liang-Chiao Huang was born in Changhua, Taiwan. He has received the B.S. and M.S. degrees in electrical engineering from National Taiwan University of Science and Technology, Taipei, Taiwan, in 2002 and 2004. From 2005 until now, he is a researcher who focused on the research of motor control of power saving in the Green Energy and Environment Research Laboratories, Industrial Technology Research Institute (ITRI), Hsinchu, Taiwan. His areas of research interests are PMSM motor control, the application of the DSP and FPGA in motor and digital power control system.